Materials Today Bio 23 (2023) 100816

Contents lists available at ScienceDirect

Materials Today Bio

journal homepage: www.journals.elsevier.com/materials-today-bio

CXCL chemokines-mediated communication between macrophages and BMSCs on titanium surface promotes osteogenesis via the actin cytoskeleton pathway

Yayun Zhang [a,b,1], Jiemao Wei [a,1], Xingbang Yu [a], Liangxi Chen [a], Ranyue Ren [a], Yimin Dong [a], Sibo Wang [a], Meipeng Zhu [a], Nannan Ming [c], Ziwei zhu [a], Chenghao Gao [a,**], Wei Xiong [a,*]

[a] Department of Orthopedic Surgery, Tongji Hospital, Tongji Medical College, Huazhong University of Science & Technology, 1095 Jiefang Avenue, Wuhan, Hubei, 430030, China

[b] Trauma Center/Department of Emergency and Trauma Surgery, Tongji Hospital, Tongji Medical College, Huazhong University of Science and Technology, 1095 Jiefang Avenue, Wuhan, Hubei, 430030, China

[c] The State Key Laboratory of Refractories and Metallurgy Institute of Advanced Materials and Nanotechnology Wuhan University of Science and Technology, Wuhan, 430081, China

ARTICLE INFO

Keywords:
Bone mesenchymal stem cells
Macrophages
Chemokines
Osteointegration
Cell-cell communication

ABSTRACT

The refined functional cell subtypes in the immune microenvironment of specific titanium (Ti) surface and their collaborative role in promoting bone marrow mesenchymal stem cells (BMSCs) driven bone integration need to be comprehensively characterized. This study employed a simplified co-culture system to investigate the dynamic, temporal crosstalk between macrophages and BMSCs on the Ti surface. The M2-like sub-phenotype of macrophages, characterized by secretion of CXCL chemokines, emerges as a crucial mediator for promoting BMSC osteogenic differentiation and bone integration in the Ti surface microenvironment. Importantly, these two cells maintain their distinct functional phenotypes through a mutually regulatory interplay. The secretion of CXCL3, CXCL6, and CXCL14 by M2-like macrophages plays a pivotal role. The process activates CXCR2 and CCR1 receptors, triggering downstream regulatory effects on the actin cytoskeleton pathway within BMSCs, ultimately fostering osteogenic differentiation. Reciprocally, BMSCs secrete pleiotrophin (PTN), a key player in regulating macrophage differentiation. This secretion maintains the M2-like phenotype via the Sdc3 receptor-mediated cell adhesion molecules pathway. Our findings provide a novel insight into the intricate communication and mutual regulatory mechanisms operating between BMSCs and macrophages on the Ti surface, highlight specific molecular events governing cell-cell interactions in the osteointegration, inform the surface design of orthopedic implants, and advance our understanding of osteointegration.

1. Introduction

Titanium (Ti) and its alloys are widely used in orthopedic implants [1,2] due to their exceptional mechanical properties, chemical stability, and biocompatibility [3,4]. A key objective in modifying Ti prostheses is to enhance the structural and functional connection between the implant surface and bone tissue, a process known as osseointegration. Numerous studies have elucidated the close relationship between osseointegration and the immune environment surrounding the implant [5–7]. Maintaining an equilibrium between the foreign body response (FBR) and tissue healing is crucial for optimal osseointegration [8], as disequilibrium can lead to subpar osseointegration and infection [9].

Macrophages and neutrophils have been identified to possess osteogenic effects [10–13]. Macrophages exhibit plasticity and are often classified into M1 and M2 subtypes [14,15]. While M1 macrophages promote inflammation responses [16], M2 macrophages exert

* Corresponding author. Department of Orthopedics, Tongji Hospital, Tongji Medical College, Huazhong University of Science and Technology, Wuhan, 430030, Hubei, China.

** Corresponding author. Department of Orthopedics, Tongji Hospital, Tongji Medical College, Huazhong University of Science and Technology, Wuhan, 430030, Hubei, China.

E-mail addresses: chenghaotj@126.com (C. Gao), xcxgreatwellus@hotmail.com (W. Xiong).

[1] The first two authors contributed equally to this study.

https://doi.org/10.1016/j.mtbio.2023.100816
Received 10 June 2023; Received in revised form 6 September 2023; Accepted 22 September 2023
Available online 5 October 2023

anti-inflammatory effects and promote tissue healing [17,18]. This biological heterogeneity can result in different osseointegration outcomes [19–21], which could be attributed to macrophages occupying distinct phenotypic states or plasticity. Previous studies have shown that altering biomaterial surface properties, such as hydrophilicity, roughness [22]], and size [23], and incorporating certain metal elements, such as Fe2+ [24], Sr2+ [25], Ag2+ [3], and Mg2+ [26], can induce diverse macrophage phenotypes and promote bone healing [27]. It is evident that macrophage phenotypes in this process appear to be far from uniform, with environmental factors seemingly driving their diverse range. M2 macrophages are more of a general definition, with more precise functional subtypes in specific microenvironments [28].

BMSCs play a pivotal role in osseointegration and are regulated by the immune system, exhibiting immunomodulatory behaviors. For instance, one study revealed BMSCs' responsiveness to immunomodulatory regulation via soluble factors like PGE2 and TSG-6 [29], while other studies suggested a direct relationship between macrophages-secreted BMP-2 and BMSC osteogenic differentiation [30,31]. Investigations into in vivo bone defects and fracture healing have elucidated the impacts of intercellular communication between macrophages and BMSC on the fate of interstitial progenitors, with specific signaling molecules such as CCL2, CXCL8, and SDF-1 varying with the experimental design and model specification [32]. These findings underscore the potential to induce specific functional macrophage phenotypes in distinct microenvironments. Nonetheless, the mutual regulation between macrophages and BMSCs within a particular host-implant interface microenvironment has yet to be thoroughly elucidated. Recent advancements in high-throughput sequencing technologies, including single-cell sequencing, have enabled more refined phenotypic identification of macrophages. Utilizing advanced bioinformatic analysis, which has been applied across various diseases [33] but rarely to periprosthetic cells, allows inference of functional macrophages in specific environments and identification of relevant functional molecules.

To accurately mimic the native environment and unravel the communication mechanisms underlying microenvironment-mediated macrophage-mesenchymal stem cell interaction, co-culture models are often employed [34]. While prior studies have established various co-culture models, such as 3D-scaffolds [35], *trans*-well insert systems [36], mini-pillar chips [37,38], 3D-spheroids [39], and indirect co-cultures [40], many of these designs are static or pertain to a single cell type, overlooking the dynamic feedback and crosstalk between main cell types on Ti prosthesis surfaces. In this study, we constructed a temporal dynamic co-culture model to investigate the interaction between BMSCs and macrophages. Through RNA sequencing and related in vivo and *in vitro* experiments, we evaluated the role of different types of macrophages in promoting osteogenesis and examined the biological interactions between BMSCs and macrophages on Ti surfaces. Our findings may provide further insights into cell subtypes and molecular mechanisms relevant to Ti interface osseointegration, guiding the design and development of novel bio-functional Ti prosthesis materials.

2. Materials and methods

2.1. Sample preparation

Titanium foils of average dimensions of 20.0 mm × 20.0 mm × 1.0 mm and 10.0 mm × 10.0 mm × 1.0 mm and titanium rods with a diameter of 1.0 mm, length of 8 mm, and purity of 99.7 % (Aldrich, USA) were polished using SiC (silicon carbide) sandpapers. Subsequently, the foils were ultrasonically cleaned for 10 min at a frequency of 100 Hz, followed by rinse in turn with acetone, ethanol (>99.7 %), and deionized water (DI). All materials were sterilized by high-pressure steam before commencing experimental procedures.

2.2. Surface characteristic

A field emission scanning electron microscope (FE-SEM) (FEI Nova 400 Nano) and an Energy- Dispersive X-ray Spectrometer (EDX, Nova Nano 450, Thermo FEI, USA) were used to observe the surface morphology and elemental composition of the Ti samples, respectively.

2.3. Isolation of BMSCs and bone marrow macrophages (BMMs)

BMSCs were isolated from the femur and tibia of 4-week-old (60–80g) male Sprague-Dawley (SD) rats. The cells obtained from the marrow cavity were cultured in the F12 medium containing 10 % fetal bovine serum in a 10 cm petri dish. After 24 h, the supernatant suspension was removed, and the adherent cells were retained and cultured by replenishing the medium every three days. Cells of three to five passages were used as BMSCs in the subsequent experiments.

BMMs were also derived from the femur and tibia of 4-week-old (60–80g) male SD rats. Cells from the marrow cavity were cultured in alpha-modified eagle medium (α-MEM, Gibco), supplemented with 10 % fetal bovine serum and 50 ng/mL macrophage colony-stimulating factor (M-CSF). After 16 h, the supernatant suspension was transferred to another 10 cm petri dish, while the adherent cells after 24 h were considered as BMMs and were further cultured with regular medium refreshing every two days. Primary BMMs were utilized for the subsequent experiments.

2.4. Co-culture of BMMs and BMSCs

BMSCs were seeded onto a designated Ti plate, whereas BMMs were seeded onto another. Upon cell attachment, the two Ti plates were placed in the same culture dish to enable co-culture. In the control group, the two cell types were cultured separately on the Ti surface in osteoblast induction media (OriCell, RAXMX-90021) for 7 consecutive days. M-CSF (50 ng/mL) was additionally supplemented in the subset involving macrophages.

2.5. RNA isolation and quantitative real-time PCR (qRT-PCR)

Total RNA was isolated using TRIzol reagent (Invitrogen, USA), and cDNA was synthesized from 1000 ng of total RNA using the Revert Aid First Strand cDNA Synthesis Kit (Hifair® III 1st Strand cDNA Synthesis SuperMix, YEASEN, China) according to the manufacturer's instructions. Hieff® qPCR SYBR Green Master Mix (No Rox) (YEASEN, China) was used for qRT-PCR. The primer sequences used for qRT-PCR are listed in Table 1.

2.6. Western blotting analyses

Western blot was employed to identify osteogenic markers, including ALP (Abcam, UK), RUNX2 (CST, USA), and OPN (Abcam, UK) in BMSCs, polarization indexes, including iNOS (Proteintech, China), TNF-a (Proteintech, China), Arg1 (CST, USA), and CD206 (Abcan, UK) in BMMs within co-culture model, and other indexes, including IL10 (Proteintech, China), CXCL3 (Abcam, UK), CXCL6 (Abclonal, China), CXCL14 (Abcam, UK), Sdc3 (Abclonal, China), Cldn1 (Abcam, UK), Itgaαl (Abclonal, China), CXCR2 (Abclonal, China), CCR1 (Abcam, UK), Pfn2 (Abclonal, China), and PTN (Abcam, UK). Cells were lysed in RIPA lysis buffer to extract total proteins. The proteins were separated by 10 % or 12 % sodium dodecyl sulfate-polyacrylamide gel electrophoresis and subsequently transferred onto PVDF membranes (0.2um, Millipore, Billerica, MA, USA). The membranes were blocked with 5 % bovine serum albumin or non-fat dry milk in TBST for 60 min at room temperature to block nonspecific binding and then incubated overnight with the primary antibodies under gentle shaking at 4 °C. The membranes were then washed three times and incubated with secondary antibodies for 1 h at room temperature. After three subsequent washes with TBST,

Table 1
Primers used for qRT-PCR.

Gene	Gene forward primer sequence (5–3)	Gene forward primer sequence (3–5)
ALP	CCAAAGGCTTCTTCTTGCTAGTG	TGATCAGCAGTAACCACAGTCAA
Runx2	GGCCACTTACCACAGAGCTATTA	GTGTCTGCCTGGGATCTGTAATC
OPN	GAGAGCGAGGATTCTGTGAACTC	CTCATCTGTGGCATCGGGATACT
OCN	GGTGCAGACCTAGCAGACACCA	AGGTAGCGCCGGAGTCTATTCA
iNOS	AATCTTGGAGCGAGTTGTGG	CAGGAAGTAGGTGAGGGCTTG
TNF-α	CCCCGACTATGTGCTCCTCAC	AGGGCTCTTGATGGCGGA
Arg1	CTCCAAGCCAAAGTCCTTAGAG	AGGAGCTGTCATTAGGGACATC
CD206	GACAGATATGAACAAGCATTCC	TGAACATCTGAGAGTCCTGTC
Ccr1	CTCTCAAAGGCCCAGAAACAAAG	GGAACTGGTCAGGAACAATAGCT
Cxcr2	AGCTGTCTCACTTTCTTCCAGTT	CCACCCTGATTTCTCCCATCTTT
Cyfip2	GCTGACCAGATCTTTGCCTACTA	TGCGTGATGAGTCTGTTCAAGTC
Itgαl	GCCCAAGACATAACCCGCTATAT	TCAGCTTCTCAAATGTGTCCAGA
Nckap1	CTCAGAGCACATGTCAGGAAGTA	TCTTCAGGGCAAACAGAGAGATT
Pfn2	GTTGGCAGAGCTACGTGGATAAC	CATCTATTTCTGCTGGCGTGATG
Ptn	CGAGTGCAAACAAACCATGAAGA	GTTCTGGTCTTCAAGGCGGTATT
Cxcl1	CTGCACCCAAACCGAAGTCATAG	CCATCGGTGCAATCTATCTTCTTTTC
Cxcl3	TTTGAGAACATCCAGAGCTTGAC	AGCTTGAGGGTTGAGACAAACTT
Cxcl6	CATTTCTGCTGCTGTTCACACTG	AGCTTCTGGGTCAAGACAAACAT
Cxcl12	CGCACTTTCACTCTCCGTCC	TGGCTCTCAAAGAATCGGCA
Cxcl14	GACGTGAAGAAGCTGGAAATGAA	CAAGATCGTCCACCCTACTCTTC
Ccl20	CCTCAGCCTAAGAACCAAGAAGAT	CACTGGGACACAAATCAGGTCTG
Cldn1	TGGGGACAACATCGTGACTG	CCCCAGCAGGATGCCAATTA
Itgα8	AGAAGACGGTCACTGTTCGAAAT	TTGATGTCTGTCAGGGCACTTAT
Sdc3	GATCTTGAGGGCTCAGGGGA	GAACCGCATGGCTGTCTCAA
GAPDH	GAAGGTCGGTGTGAACGGAT	CCCATTTGATGTTAGCGGGAT

images were captured via enhanced chemiluminescence (Thermo Fisher Scientific) and quantified using Image Lab 5.1 software (Bio-Rad, Hercules, CA, USA).

2.7. Immunofluorescence analysis

Cells cultured separately and co-cultured on titanium sheets were fixed with 4 % paraformaldehyde for 15 min. After permeabilization using 0.2 % Triton X-100 (Solarbio) for 10 min, cells were incubated with 1 % BSA in PBST at room temperature for 30 min to block nonspecific binding. Subsequently, cells were incubated with diluted primary antibodies overnight at 4 °C, followed by three washes with PBS. Then, the cells were incubated with secondary antibodies in the dark for 1 h and counterstained with DAPI (Solarbio) for 5 min. The resultant images were captured using a fluorescence microscope.

2.8. Implantation model

All the experiments were approved by the Institutional Animal Ethics Committee of Tongji Hospital, Tongji Medical College, Huazhong University of Science and Technology, Wuhan, China (TJH-202101004). To evaluate changes in the surrounding immune environment and bone healing after implantation, we established a femoral defect model in male SD rats. Thirty-two male SD rats (150 ± 20 g, 5-week-old) were procured from the Experimental Animal Center of Tongji Hospital (Wuhan, China) and acclimated in the laboratory under standard conditions for 1 week. These rats were then randomly allocated into 2 groups (Titanium rods group and Blank control group, n = 16), with each group further divided into 4 subgroups (n = 4) corresponding to post-surgery durations of 3, 7, 14, or 28 days. Prior to the procedures, all rats were anesthetized using pentobarbital. An incision was made through the skin and subcutaneous tissues along the medial femur on both sides to expose the epiphyseal bone surface. Utilizing an electric drill, a hole of 2 mm diameter was drilled perpendicular to the bone surface for implanting titanium rods. The incision was subsequently sutured in layers, and each rat received a 0.5 mL antibiotic dose to prevent infection. At the end of the experiment, all rats were euthanized, and samples of the soft tissue surrounding the defect and the femur were collected for subsequent analysis.

2.9. H&E staining and immunohistochemistry

Fresh tissues were fixed for more than 24 h, embedded in paraffin, and sectioned at a thickness of 4 μm. These sections were subjected to hematoxylin and eosin (H&E) staining and immunohistochemical staining. The staining results were observed and recorded under a microscope.

2.10. Micro-CT analysis

The collected bilateral femurs were fixed in 4 % paraformaldehyde for 2 days. Subsequently, distal femurs were scanned using a high-resolution Micro-CT with scanning parameters setting as follows: source voltage at 70 kV, source current at 114 μA, and isotropic resolution at 20 μm. The built-in software of Micro-CT was employed for bone morphologic analysis and 3D reconstruction based on morphologic parameters, including bone volume/tissue volume (Bv/Tv), trabecular thickness (Tb.Th), trabecular number (Tb.N), and trabecular distance (Tb.Sp).

2.11. RNA sequencing and data analysis

BMMs and BMSCs were cultured separately or co-cultured for four days. Following this, RNA was extracted using TRIzol reagent (Invitrogen, USA) and submitted to Novogene (Beijing, China) for RNA sequencing. Differentially expressed genes (DEGs) between the separate and co-culture groups of BMMs and BMSCs were identified based on the threshold of |log2(Foldchange)| of 0.5. These DEGs were further subjected to analysis using the Kyoto Encyclopedia of Genes and Genomes (KEGG), Gene Ontology (GO), and protein-protein interaction (PPI) networks to unravel potential mechanisms underlying their communication.

2.12. ELISA

Proteins secreted by the two types of cells in the co-culture model were detected using CXCL3 and PTN ELISA Kits from JiangLai Biological (Shanghai, China) and CXCL6 and CXCL14 ELISA Kits from Cloud-Clone Corp (Wuhan, China).

2.13. Cytotoxicity assay

The cytotoxicity and proliferation effects of CXCL3, CXCL6, and CXCL14 on BMSCs and PTN on BMMs were determined using the CCK-8 kit. After attachment, cells (5×10^3/well) in 96-well plates) were treated with various concentrations of CXCL3, CXCL6, CXCL14, and PTN with replicates for each concentration. Upon the completion of the intervention, 10 μL of CCK-8 solution was added to each well. After incubation at 37 °C for 1 h, the absorbance at 450 nm was measured using a plate reader.

2.14. Pfn2 knockdown using small interfering RNA

Small interfering RNA was used to knock down Pfn2. In brief, 5 μL of small interfering RNA (Si-Pfn2, sense: GCAAAAUACUUGAGAGACUTT, antisense: AGUCUCUCAAGUAUUUUGCTT) was mixed with 5 μL of Lipo-3000n (Thermo, USA) in 120 μL of opti-MEM (Gibco, USA). After incubation at room temperature for 15 min, the mixture was added to 1750 μL of F12 medium and used to culture BMSCs for 24 h in 6-well plates.

2.15. Statistical analysis

Statistical analysis was performed using GraphPad Prism 9.0 (GraphPad Software, San Diego, CA, USA). Differences between two groups were analyzed using a two-tailed student t-test and differences among multiple groups were analyzed using a one-way analysis of variance (ANOVA). Data were expressed as mean ± standard error of the mean (SEM). All data were obtained from at least three independent experiments. $^*P < 0.05$, $^{**}P < 0.01$, $^{***}P < 0.001$, and $^{****}P < 0.0001$.

3. Results

3.1. Material microstructure, elemental analysis, and construction of co-culture model

We employed a titanium alloy as the substrate for cell culture. All materials were synthesized in a consistent way to ensure uniform morphological characteristics. The surface microstructure and morphology were observed using FE-SEM (Fig. 1A and B). Concurrently, the element composition of the materials was examined using EDX. Notably, apart from the artificially sprayed Au element, Ti element stands out as the principal constituent element of the material, as demonstrated in Fig. 1C. We established a direct co-culture model to explore the interactions between BMSCs and BMMs following the intervention of Ti materials. Specifically, BMSCs and BMMs were seeded separately on Ti plates and transferred to the same culture dish for co-culture (Fig. 1D).

3.2. Co-culture triggers M2-like phenotype transformation of BMMs and enhances osteogenic differentiation of BMSCs

Firstly, we investigated the effects of Ti on macrophages. The results showed that Ti exposure led to an elevated mRNA level of the M1-like (pro-inflammatory) marker *iNOS* across all observed time points but a reduction in the mRNA level of the M2-like (anti-inflammatory) marker *CD206* at 4 and 7 days when compared to the control group. These findings imply that the involvement of Ti triggers BMMs to polarize towards the M1-like phenotype (Fig. 2A). Then, we examined the effects of Ti intervention on BMMs during co-culture with BMSCs. The results showed a significant time-dependent increase in the mRNA level of the M2-like markers *CD206* and Arg1 within co-cultured BMMs. Conversely, we observed a significant decrease in the mRNA level of the M1-like markers *iNOS* and *TNF-α* (Fig. 2B). These observed patterns were mirrored in the protein levels of these markers (Fig. 2C and D). Further exploration using immunofluorescence analysis of BMMs confirmed that M1-like markers were highly expressed in separate culture conditions,

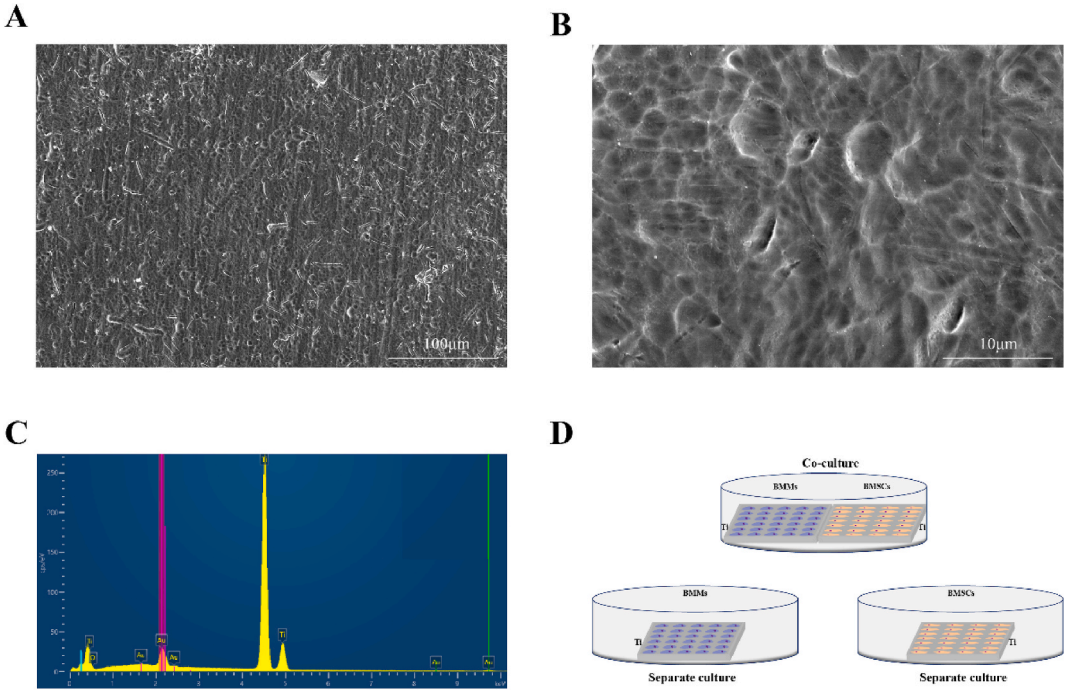

Fig. 1. Microstructure and co-culture model construction. (A and B) The surface morphology of the sample was observed using FE-SEM after gold spraying at a scale of 100 μm (A) and 10 μm (B). (C) The element composition of the sample was analyzed using EDX, with Ti as the predominant element composition. (D) Co-culture model. BMSCs and BMMs were separately cultured on Ti plates, and the attached cells were transferred to the same culture dish for co-culture.

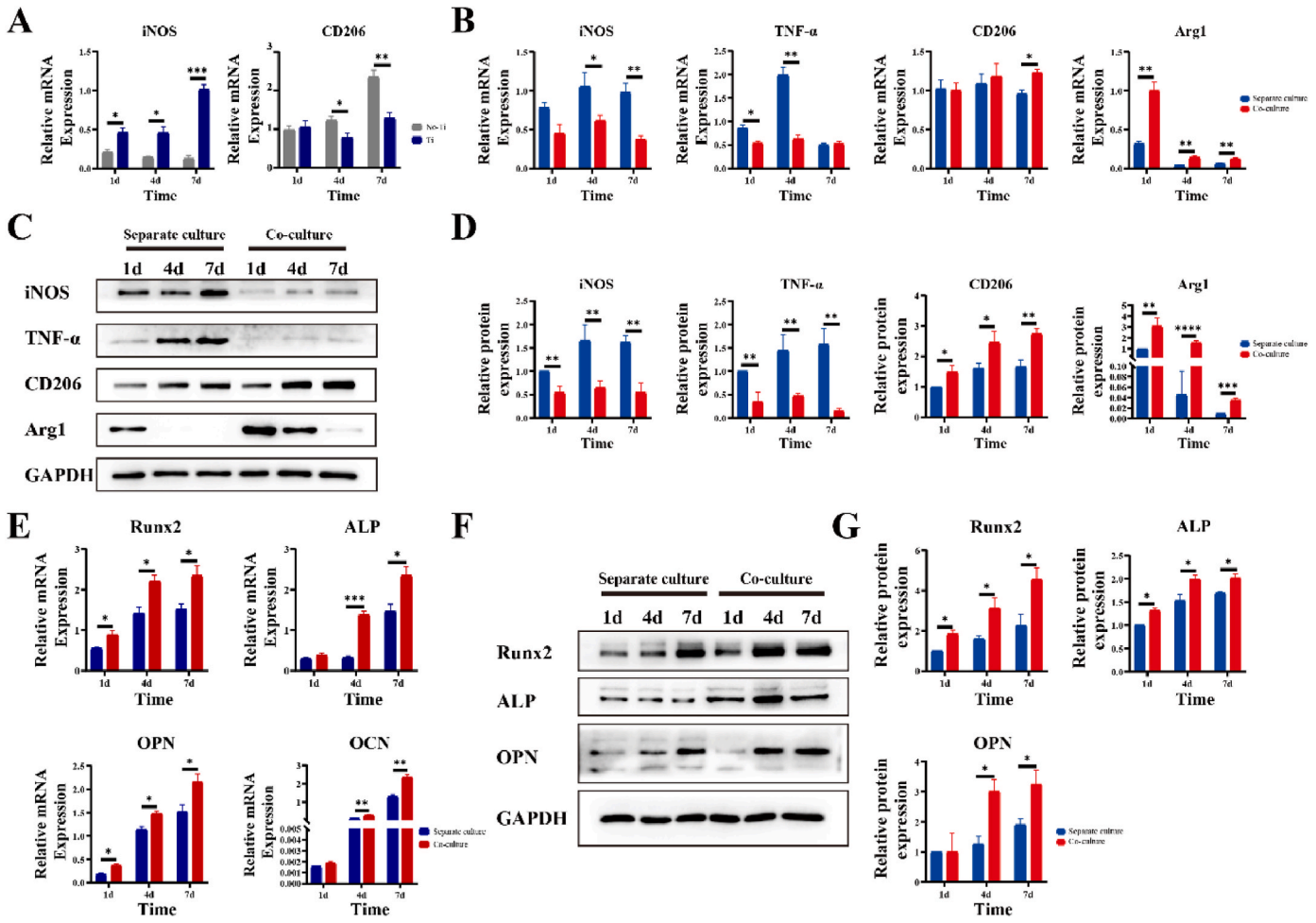

Fig. 2. Effects of Ti on BMMs and temporal changes in BMMs and BMSCs in the co-culture model. (A) BMMs have distinct phenotypes with and without Ti intervention. Changes in mRNA expression were detected at various time points. (B, C, D) The time-dependent changes in polarization-related genes of BMMs at both mRNA and protein levels across separate culture and co-culture groups. (E, F, G) The time-dependent changes in osteogenesis-related genes of BMSCs at both mRNA and protein levels cross in separate culture and co-culture groups. Data are presented as the mean ± SEM of at least three independent experiments. $*p < 0.05$, $**p < 0.01$, $***p < 0.001$, and $****p < 0.0001$. mRNA and protein expression levels were normalized to that of separate culture on day 1.

while M2-like markers were highly expressed in co-cultured BMMs at various time points (Fig. S1).

Subsequently, we detected the expression of osteoblast-related genes in BMSCs in the co-culture system, including *RUNX2*, *ALP*, *OPN*, and *OCN*. The results showed that expression of all these genes in the co-culture system increased at both mRNA and protein levels over time compared to the separate culture system (Fig. 2E, F, and G).

In conclusion, the co-culture-induced phenotype of BMMs exhibited a promotive effect on the osteogenic differentiation of BMSCs compared to the separate culture.

3.3. *In vivo implantation of Ti rod did not affect the bone formation and M2-like differentiation of macrophages around the defect*

Bilateral distal femurs of SD rats were utilized to construct bone defects, followed by implanting Ti rods. DR imaging showed appropriate implant positioning (Fig. 3A). The rats were observed at 3, 7, 14, and 28 days post-Ti rod implantation. At the 3-day-post Ti rod implantation, immunofluorescence demonstrated the deposition of BMMs (green) and BMSCs (red) on the Ti surface (Fig. 3B), indicating the interaction between BMMs and BMSCs on the Ti surface in an in vivo microenvironment. Consequently, femurs from the SD rats were collected at each time point for CT analysis and reconstruction observation. Over time, a concentric encirclement of new, dense bone tissue around the Ti rod was evident (Fig. 3C). Bone morphological parameters, including BV/TV, Tb.Th, Tb.N, and Tb.Sp, were quantified. In comparison to the control group, minimal variations were observed on day 3. However, significant decreases on day 7 and significant increases on days 14 and 28 were observed in BV/TV, Tb.N, and Tb.Th. In contrast, an inverse trend was observed in Tb.Sp (Fig. 3D). These changes in bone morphological parameters over time indicated robust osseointegration after Ti rod implantation.

H&E staining of the soft tissue surrounding the defects post Ti rod implantation revealed substantial infiltration of cells on days 3 and 7. Over time, the number of infiltrating cells surrounding the soft tissue decreased (Fig. 3E). Immunohistochemical staining verified the presence of BMMs in the surrounding soft tissues and the temporal changes in macrophage phenotypes. Moreover, significant expression of the M1-like markers iNOS and TNF-α and M2-like markers Arg1 and CD206 were observed at day 3. However, the expression levels of M2-like markers Arg1 and CD206 were significantly higher than that of the M1-like markers iNOS and TNF-α at day 7 (Fig. 3F), indicating that BMMs proximal to the Ti implant exhibited a gradual transition towards the M2-like phenotype over time.

We further analyzed protein levels in the soft tissues surrounding the Ti rod to evaluate macrophage changes at the protein level. The results showed macrophage invasion was most prominent at the initial phase, intensifying within 7 days before precipitously declining post this

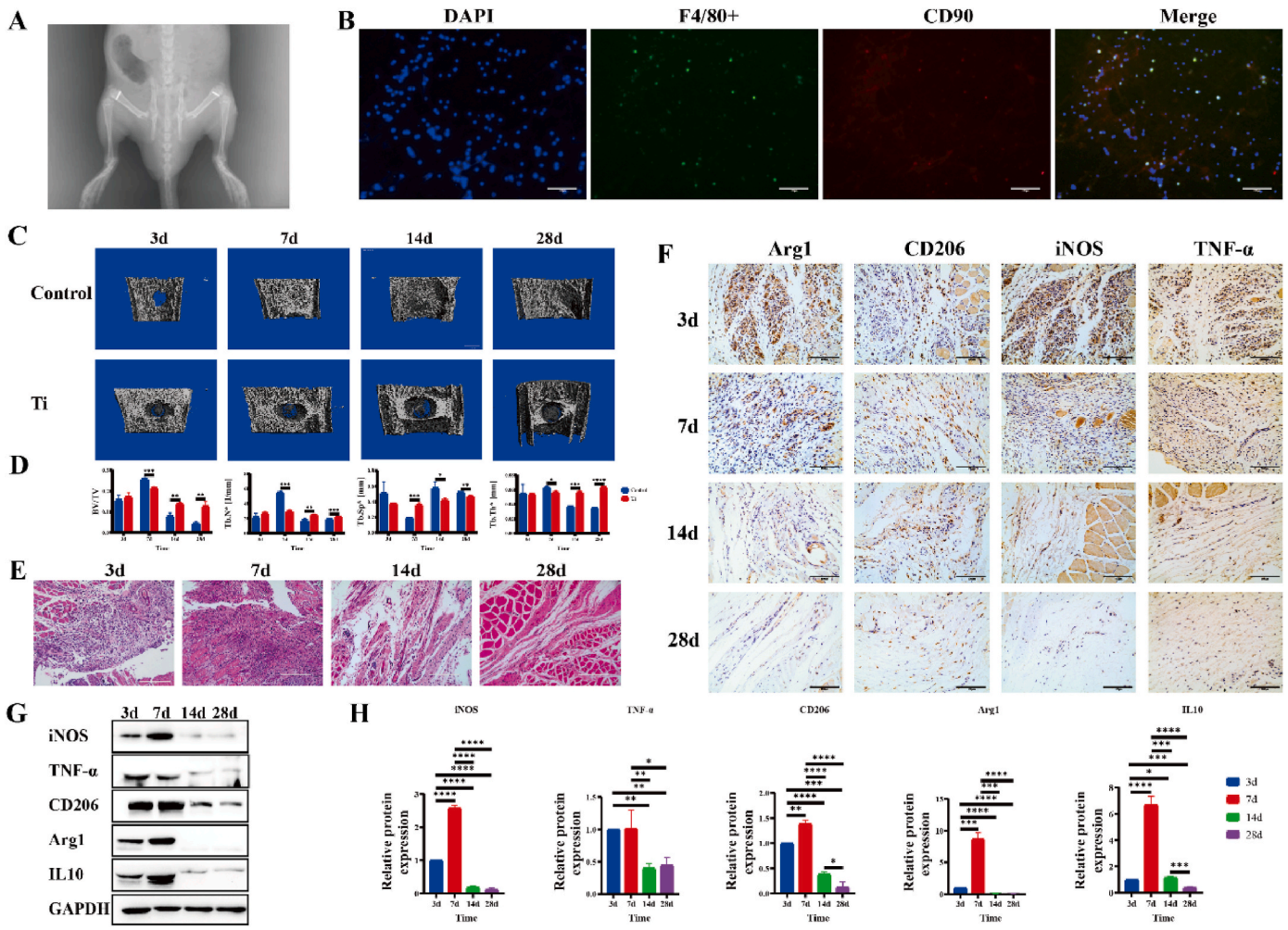

Fig. 3. *In vivo* alterations in osteogenesis and immune environment after Ti rod implantation. (A) Images of the implanted Ti rods captured using DR. (B) Immunofluorescence imaging of BMMs (F4/80+) and BMSCs (CD90) on the Ti surface at the juncture on day 3 of post-Ti rod implantation. (C) Three-dimensional reconstruction encircling the femur at various time points post-Ti rod implantation. (D) levels of bone structure-related parameters, including BV/TV, Tb.N, Tb.Sp, and Tb.Th; (E) H&E staining of the neighboring soft tissues of the femur at various time points. (F) Immunohistochemical staining of Arg1, CD206, iNOS, and TNF-α in the soft tissues surrounding the femur modeling at various time points. (G, H) Expression of tissue proteins related to macrophage polarization at various time points, including Arg1, CD206, IL-10, iNOS, and TNF-α. Data are presented as mean ± SEM of at least three independent experiments. $*p < 0.05$, $**p < 0.01$, $***p < 0.001$, and $****p < 0.0001$. The protein expression was normalized to the control group on day 3.

duration (Fig. 3G and H). Overall, our in vivo experiments support the results of our *in vitro* cell experiments and validate the rationality of the intervention timing we established in our *in vitro* cell experiments.

3.4. RNA-seq reveals increased expression of chemokines and related pathway genes in BMMs and upregulation of PTN, receptors, and related pathway genes in BMSCs

To further explore the mechanisms underlying the interaction between BMMs and BMSCs in the co-culture system on Ti surface, we performed whole genome RNA sequencing on BMMs and BMSCs after 4 days of co-culture. Initially, we analyzed DEGs in BMMs during co-culture with BMSCs (Fig. 4A). Using KEGG pathway enrichment analysis, we identified the top 20 signaling pathways with the most significant differences (Fig. 4B). The Venn diagram showed the distinct gene count in separate culture and co-culture systems (Fig. S2A). GO analysis revealed ten signal pathways with the most significant differences across biological process (BP), cell component (CC), and molecular functions (MF) (Fig. 4C and S2B). Within the MF-focused GO analysis, the trajectory of BMMs' changes culminated in the chemokine activity pathway. The quantification of upregulated genes post-co-culture was depicted (Fig. 4D). PPI analysis of aforementioned chemokines indicated that their corresponding receptors CXCR2 and CCR1 were among the DEGs in BMSCs (Fig. 4E) and enriched in the transmembrane signaling receptor activity pathway. PPI analysis also revealed genes related to the receptors CXCR2 and CCR1(Fig. 4F). KEGG analysis of these genes unveiled that Itgal was enriched into the regulation of the actin cytoskeleton pathway in BMSCs. The quantification of these related upregulated genes is shown in Figs. S2C and D.

We further analyzed DEGs in BMSCs during co-culture with BMMs (Fig. 4G). KEGG pathway enrichment analysis revealed the top 20 signaling pathways with the most significant differences (Fig. 4H). The Venn diagram showed the distinct gene count in separate culture and co-culture systems (Fig. S2E). GO analysis indicated that the top ten signal pathways with the most significant differences were BP, CC, and MF (Fig. 4I and S2F). Further GO analysis of MF showed that the trajectory of BMSCs' changes culminated in the integrin binding pathway. The quantification of upregulated genes post-co-culture was depicted in Fig. 4J. Among these upregulated genes, Col4a3, Ptn, IL1β, and Fermt3 are regulators of secretory proteins. PPI analysis indicated that PTN receptor Sdc3, Ptprz1, and IL1β receptor IL1r1 were among the upregulated genes BMSCs during co-culture with BMMs (Fig. 4K). KEGG

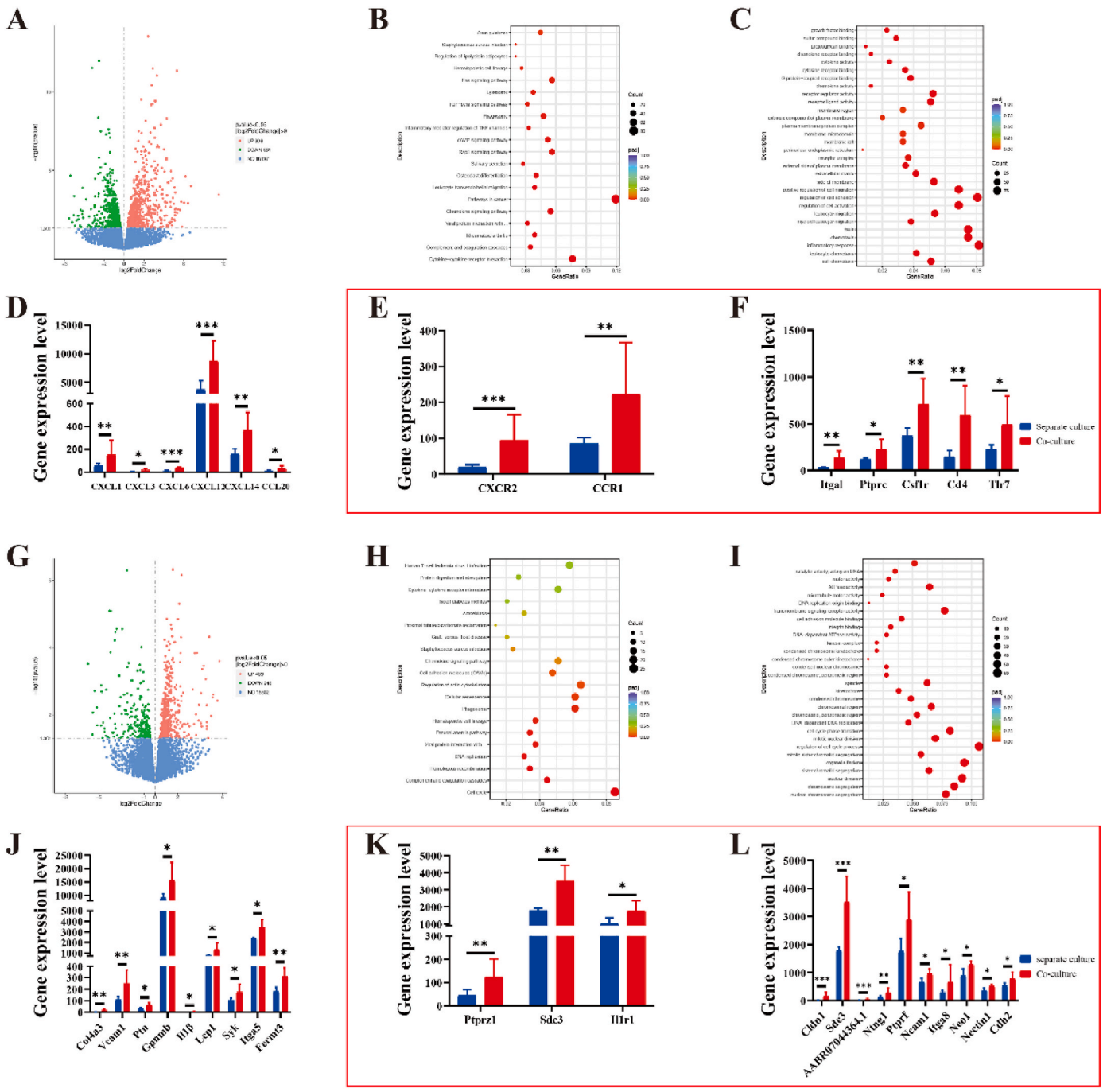

Fig. 4. Transcriptomic insights into intercellular signaling in co-culture system. RNA-seq results revealed 1) increases in BMMs-secreted chemokines under the influence of BMSCs and in expression of receptors CXCR2 and CCR1 on BMSCs, as well as activation of their downstream actin cytoskeleton pathway, and 2) increases in BMSCs-secreted PTN under the influence of BMMs and in expression of the receptor Sdc3 located on BMMs as well as activation of its downstream cell adhesion molecules. (A) The volcano plot of DEGs in BMMs in the co-culture system. (B) KEGG enrichment pathway analysis of BMMs after co-culture with BMSCs. (C) The scatter plot diagram of GO analysis of DEGs in BMMs in the co-culture system. (D) Quantified expression of upregulated chemokines secreted by BMMs in the co-culture system. (E) Expression of chemokine receptors CXCR2 and CCR1 in the separate and co-culture systems. (F) Expression of genes involved in the PPI network of chemokine receptors CXCR2 and CCR1 in the separate and co-culture system. The data in the red box were derived from RNA-seq analysis of BMSCs. (G) The volcano plot of DEGs in BMSCs the co-culture system. (H) KEGG enrichment pathway analysis of DEGs in BMSCs after co-culture with BMMs. (I) The scatter plot diagram of GO analysis of DEGs in BMSCs after co-culture with BMMs. (J) GO analysis of DEGs of BMSCs under the influence of BMMs, showing that the integrin-binding pathway was the most important pathway, and expression quantification of up regulated genes in the integrin binding pathway. (K) The expression of PTN receptors Sdc3 and Ptprz1, and the Il1β receptor Il1r1 in the separate and co-culture system. (L) Expression of genes involved in the PPI network of PTN receptors Sdc3 in the separate and co-culture system. The data in the red box were derived from RNA-seq analysis results of BMMs. Data are presented as mean ± SEM of at least three independent experiments. $*p < 0.05$, $**p < 0.01$, $***p < 0.001$, and $****p < 0.0001$.

analysis of these receptors indicated that Sdc3 was enriched into the cell adhesion molecules pathway in BMMs. Fig. 4L shows the quantification of the related upregulated genes.

Overall, our RNA sequencing disclosed augmented secretion of chemokine family molecules by BMMs in response to the influence of BMSCs. This reciprocal modulation led to the upregulation of corresponding receptors, CXCR2 and CCR1, along with downstream signaling pathways (regulation of actin cytoskeleton pathway) in BMSCs. Furthermore, under the influence of BMMs, PTN secretion by BMSCs was also increased, accompanied by the upregulation of the correspondent receptors Sdc3 and downstream signaling pathway (cell adhesion molecules pathway) in BMMs.

3.5. Interplay of chemokines and PTN between co-cultured BMMs and BMSCs via their receptors

RNA sequencing results were further verified *in vitro* at various time points. Compared with the separate culture, co-culture of BMMs and BMSCs led to a remarkable surge in the secretion of CXCL1, CXCL3, CXCL6, CXCL14, and CCL20, particularly pronounced on day one; however, CXCL12 did not exhibit a similar trend (Fig. 5A). In tandem, co-culture also significantly increased the mRNA level of chemokine receptors *CXCR2* and *CCR1* situated on BMSCs' membrane (Fig. 5B), augmented the secretion of PTN by BMSCs across all time points (Fig. 5C), and enhanced the mRNA level of PTN receptor Sdc3 on BMMs, especially on day 1 and day 4 (Fig. 5D).

Western blot analysis revealed no significant changes in the protein levels of CXCL3, CXCL6, and CXCL14 in the chemokine family during the co-culture. CXCL3 level was significantly increased on day 1, though but showed no significant changes at other time points. CXCL6 expression gradually increased over time, showing significant changes on day 4 and day 7. In contrast, CXCL14 level was significantly increased on day 4 and day 7, yet the level on day 7 was significantly lower than that on day 4 (Fig. 5E and F). Similarly, PTN content in co-cultured BMSCs surpassed that in the separate culture on day 1 and day 4, but dipped one day 7 (Fig. 5E and F). Meanwhile, we also detected the expression of

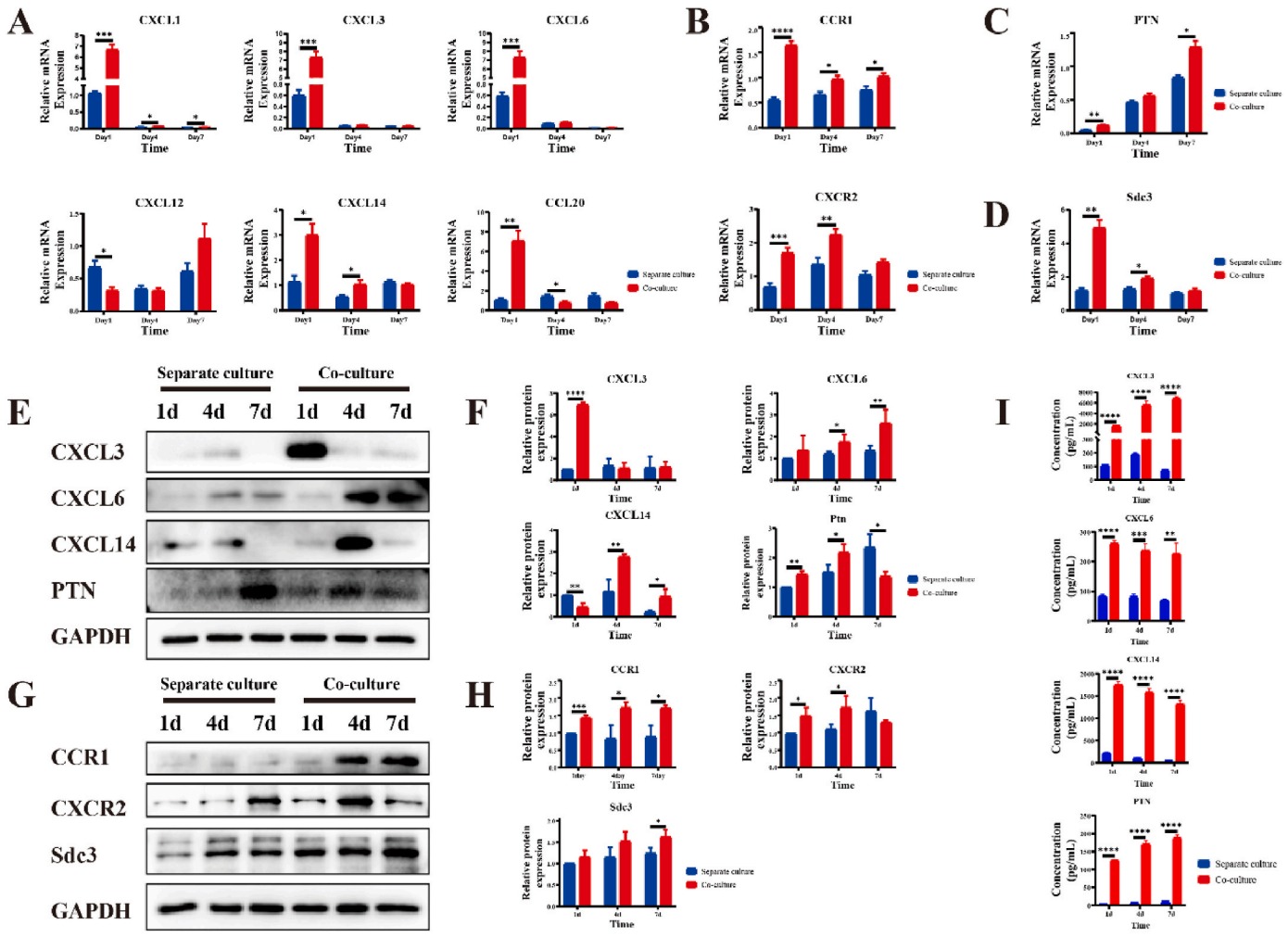

Fig. 5. Dynamic interactions between BMMs and BMSCs in the co-culture system. Under co-culture conditions, a reciprocal interplay unfolds between BMMs and BMSCs, driven by distinct signaling mechanisms. BMMs initiate changes in BMSCs by upregulating the secretion of chemokines and engaging chemokine receptors on BMSC surfaces. Conversely, BMSCs exert influence on BMMs by heightening PTN secretion and interacting with the Sdc3 receptors on BMM surfaces. (A) Temporal evolution of chemokine family-related gene expression in BMMs at mRNA levels in separate culture and co-culture systems. (B) Alterations in the expression of chemokine family-related gene receptors in BMSCs at the mRNA level in separate and co-culture systems. (C) Time-dependent shifts in PTN mRNA expression. (D) Temporal changes in PTN receptor *Sdc3* mRNA expression on macrophages. (E, F) Protein expression profiles of CXCL3, CXCL6, CXCL14, and PTN over time in separate and co-culture systems. (G, H) Dynamics of protein expression for chemokine receptors CCR1 and CXCR2, and PTN receptor Sdc3, over time in separate and co-culture systems. (I) Time-course variations in CXCL3, CXCL6, CXCL14, and PTN levels in cell supernatant observed using ELISA in separate and co-culture systems. Data are presented as mean ± SEM of at least three independent experiments. $^{*}p < 0.05$, $^{**}p < 0.01$, $^{***}p < 0.001$, and $^{****}p < 0.0001$. mRNA and protein expression were normalized to those of the separate culture system on day 1.

chemokine receptors *CXCR2* and *CCR1* on the surface of BMSCs and the level of PTN receptor Sdc3 on the surface of BMMs. The results showed that compared to the separate culture, co-culture significantly augmented the protein level of chemokine receptor CCR1 over time. In addition, co-culture also increased CXCR2 expression on day 1 and day 4, but decreased its level on day 7. Meanwhile, Sdc3 protein level in BMMs was significantly higher in the co-culture system than in the separate culture, especially on day 7 (Fig. 5G and H).

ELISA of chemokines and PTN content in cell culture medium revealed significant increases in levels of CXCL3, CXCL6, and CXCL14 secreted by BMMs and PTN secreted by BMSCs in the co-culture system at each time point (Fig. 5I).

Collectively, in the co-culture system, BMMs secreted chemokines that bound to chemokine receptors on BMSCs, thereby influencing BMSCs' function. Concurrently, PTN secreted by BMSCs interacted with the receptor BMMs' cell membranes, further influencing BMMs' function.

3.6. Reciprocal modulation of cell functions in co-cultured BMMs and BMSCs via downstream receptor signaling pathways

PPI analysis of chemokine receptors CXCR2 and CCR1 showed the enrichment of their related Itgαl in the regulation of the actin cytoskeleton pathway. In addition, Itgαl, Nckap1, Cyfip2, and Pfn2 in the co-culture system exhibited higher expression levels compared to the separate culture system, with Itgαl, Cyfip2, and Pfn2 displaying the most substantial differences (Fig. 6A). Similarly, RNA sequencing data identified Sdc3 in BMMs as enriched in the cell adhesion molecules (CAMs) pathway. Subsequent assessment of downstream molecules Cldn1 and Itgα8 in this pathway showed higher Cldn1 expression in the co-culture system, particularly on day 7. In contrast, Itgα8 expression showcased an opposite trend (Fig. 6B). The protein levels of Itgαl were also significantly higher in the co-culture system on day 1 and day 4, while no significant difference was observed on day 7. Unlike Itgαl, Pfn2 expression was consistently higher across all time points in the co-culture group (Fig. 6C and D). On day 7, CLDN1 protein level was significantly higher in the co-culture system than in the separate culture system (Fig. 6E and F).

We further explored the relationship between osteogenesis and Pfn2, which is involved in regulating actin cytoskeletal pathways. We transfected si-RNAs (Fig. 6G) specifically against Pfn2 in BMSCs and confirmed that Pfn2 expression was significantly downregulated in the si-Pfn2 group than in the control group (Fig. 6H). We then examined the effects of Pfn2 downregulation on RUNX2 and ALP, two early osteogenic

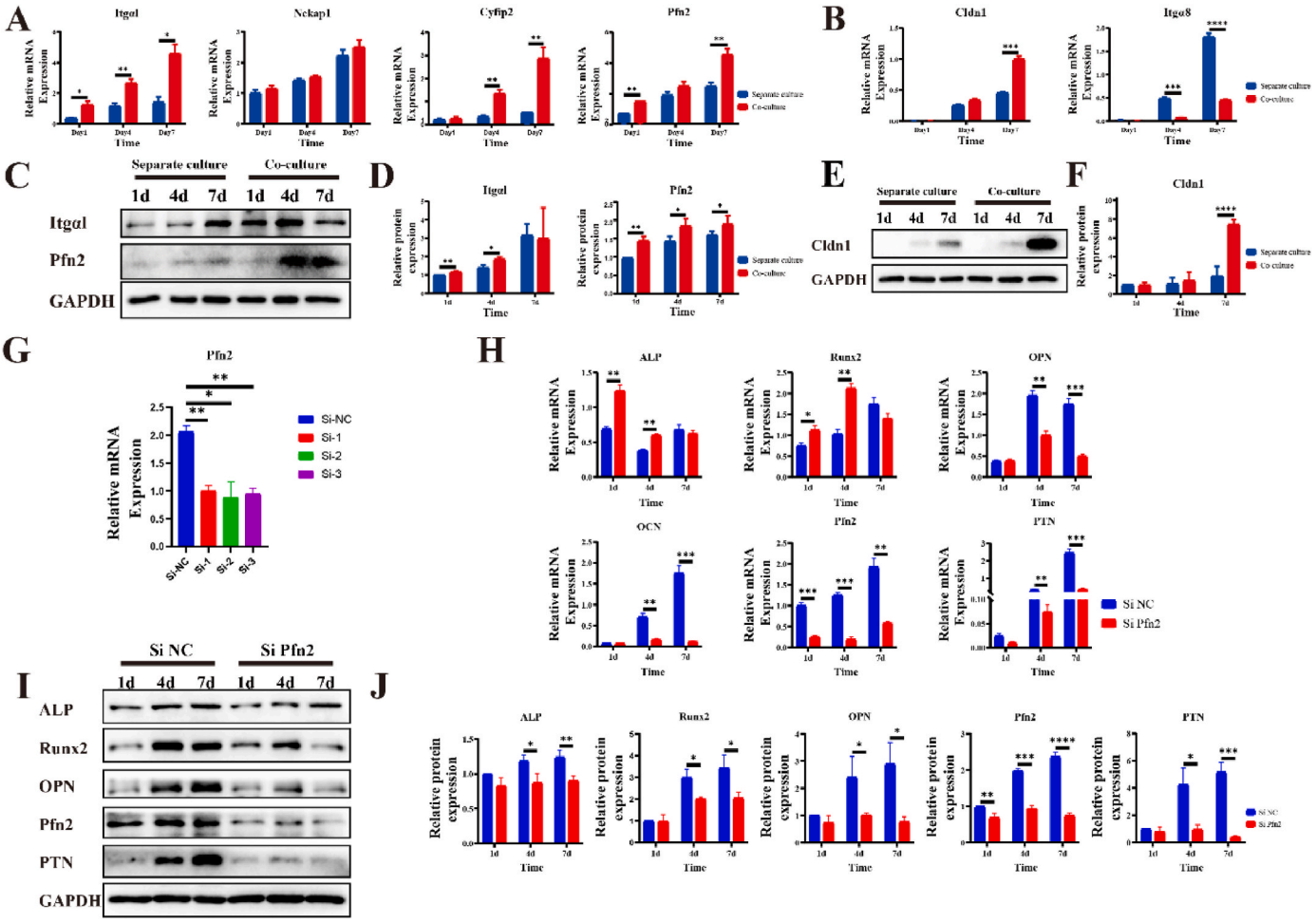

Fig. 6. Interplay of signaling pathways impacting cellular phenotypes of BMMs. The phenotypic transformations of BMMs are governed by the CAM signaling pathway. Conversely, the functional shifts of BMSCs are influenced by the regulation of the actin cytoskeleton pathway, with Pfn2 demonstrating a positive association with BMSC osteogenic differentiation. (A) Changes in mRNA levels of Itgαl, Nckap1, Cyfip2, and Pfn2 in BMSCs over time in the separate and co-culture systems. (B) Changes in mRNA level of Cldn1 and Itgα8 in BMMs over time in the separate and co-culture systems. (C, D) Time-dependent protein expression of Itgαl and Pfn2 in the separate and co-culture systems. (E, F) Time-dependent protein expression of Cldn1 in the separate and co-culture systems. (G) Pfn2 mRNA expression in BMSCs after two days of si-Pfn2 interference. (H, I, J) Expression of osteoblast-related genes and corresponding regulatory molecules in BMSCs at various time points with or without si-Pfn2 interference at both mRNA and protein levels. Data are presented as mean ± SEM of at least three independent experiments. $*p < 0.05$, $**p < 0.01$, $***p < 0.001$, and $****p < 0.0001$. mRNA and protein expression levels were normalized to those of the si-NC group on day 1.

differentiation indicators, and OPN and OCN, two late osteogenic differentiation indicators. The results showed higher RUNX2 and ALP mRNA levels in the si-Pfn2 group than in the control group on day 1 and day 4, but lower RUNX2 and ALP mRNA levels on day 7. Conversely, OPN and OCN mRNA levels were significantly lower in the si-Pfn2 group than the control group on day 4 and day 7. We also detected the protein expression of osteoblast genes in BMSCs after Pfn2 downregulation and found that RUNX2, ALP, and OPN protein levels were significantly lower in the si-Pfn2 group than in the control group on day 4 and day 7, while PFN2 protein levels were lower in the si-Pfn2 group than in the control group across all time points (Fig. 6I and J).

Collectively, these results indicate that BMMs undergo M2-like polarization due to PTN stimulation via the CAMs pathway in the co-culture system. By contrast, chemokine-driven activation of BMSCs spurs osteogenic differentiation via the regulation of the actin cytoskeleton pathway, with Pfn2 exhibiting a positive correlation with BMSC osteogenic differentiation.

3.7. Reciprocal regulation of chemokines and PTN in BMSCs and BMMs

To verify the effects of CXCL3 on BMSCs, we utilized synthetic CXCL3 proteins to intervene BMSCs. The optimal stimulus concentration of CXCL3 proteins for BMSC proliferation was 50 ng/mL, as determined using the CCK-8 kit (Fig. 7A). Following CXCL3 intervention, the mRNA expression of osteoblast-related genes increased with time at a significant level, especially for *OPN* and *OCN* (Fig. 7B). Further exploration of protein expression revealed that CXCL3 intervention significantly increased the expression of osteogenic genes *RUNX2*, *ALP*, and *OPN*, as well as CXCL3 receptor CXCR2, Itgαl, Pfn2, and PTN in the BMSCs at all time points (Fig. 7C and D).

Similarly, the influence of CXCL6 on BMSCs was examined at a concentration of 50 ng/mL (Fig. S3A). Comparable to CXCL3, CXCL6 exhibited consistent osteogenic effects, promoting differentiation via binding to CXCR2 and the regulation of the actin cytoskeleton pathway over time (Figs. S3B, C, and D).

The impact of CXCL14 on BMSCs was also investigated. At a concentration of 100 ng/mL (Fig. S4A), CXCL14 exhibited short-term osteogenic effects (on day 1 and day 4), similar to CXCL3 and CXCL6. Following CXCL14 intervention, osteogenic differentiation was enhanced over time via binding to its receptor *CCR1* and regulating the actin cytoskeleton pathway. However, this trend was reversed on day 7 (Figs. S4B, C, and D).

Moreover, we also investigated the effect of synthetic PTN proteins on BMMs. The optimum stimulus concentration of synthetic PTN proteins for BMM proliferation was identified to be 100 ng/mL using the CCK-8 kit (Fig. 7E). PTN intervention significantly decreased mRNA expression of the M1-like markers *iNOS* and *TNF-α* but increased mRNA expression of the M2-like markers Arg*1* and *CD206* at each time point. Notably, PTN receptor *Sdc3* level showed significant upregulation on day 1, and *Cldn1* in the CAM pathway demonstrated elevated expression at all time points, with significant differences on day 4 and day 7. Under PTN influence, BMMs secreted more CXCL3 and CXCL6 on day 1 and day 4 but less CXCL3 and CXCL6 on day 7. CXCL14 secretion was elevated on day 1, with no significant changes at other time points (Fig. 7F). Correspondingly, protein levels of the markers of M2-like were increased, while those of M1-like markers were decreased. Furthermore, the levels of PTN receptor SDC3, its downstream CLDN1, and secreted chemokines CXCL3, CXCL6, and CXCL14 were all notably increased in comparison to the control group at all time points (Fig. 7G and H).

In conclusion, CXCL3 and CXCL6 interact with their receptor CXCR2 on BMSCs, promoting osteogenic differentiation via regulating the actin cytoskeleton pathway in a time-dependent manner. In contrast, CXCL14 exhibits a distinct pattern by promoting early-stage osteogenic differentiation of BMSCs but inhibiting it as time progresses. In addition, PTN's binding to its Sdc3 receptor on the surface of BMMs induces M2-like polarization and chemokine secretion via the CAM pathway. The intricate mechanisms of cell-cell communication on titanium surfaces are summarized in Fig. 8 (Graphical Abstract).

4. Discussion

Despite the long-standing clinical use of Ti prostheses and their generally favorable osseointegration outcomes, not all cases achieve success, and poor osseointegration remains a prevalent issue. While diverse surface modification strategies have been explored, many of them introduce undesirable biological toxicities and side effects, impeding their clinical applications [41,42]. The process of bone healing is intricately linked to the surrounding immune system [18,27]. A deeper understanding of the mechanisms underlying the interaction between immune cells and BMSCs in the prosthetic microenvironment is imperative to improve the efficacy of Ti prostheses. Previous research [43] has predominantly focused on the responses of certain cell types to prosthetic materials or their modifiers. However, the precision of these phenotypic identifications is questionable due to the reliance on consensus molecular markers. To obtain a more accurate understanding of the functional phenotype of BMMs in the Ti prosthesis microenvironment and to elucidate the significance of cell-cell communication between CXCL chemokine-secreting M2-like BMMs and BMSCs in the osteointegration process, this study employed took a comprehensive and multidisciplinary approach.

Temporal dynamic co-culture models, integrated RNA sequencing analyses, and complementary *in vitro* and in vivo experiments were collectively employed to validate novel insights. The findings suggest that the intercellular communication between CXCL chemokine-secreting M2-like BMMs and BMSCs could potentially play a pivotal role in facilitating the successful osseointegration on Ti surfaces.

BMMs are key players in shaping the surface-based immune microenvironment of Ti implants, where CXCL chemokine-secreting M2-like BMMs emerge as promising contributors to osteogenic immunity. Macrophages display innate plasticity in responding to various stimuli by polarizing to different phenotypes to perform different functions [44,45]. Generally, macrophages are categorized into classically activated macrophages (M1) and alternatively activated macrophages (M2) [46]. Despite the established role of macrophages in osteogenesis [19], the precise type of macrophages responsible for promoting osteogenic differentiation remains unclear, with some reports suggesting that M1-like macrophages support this process [20,47–49], whilst others assert that M2-like macrophages are more effective [19,21,50]. Given the contextual disparities influencing the effect of macrophages in different induction environments, the M1/M2 classification based on molecular markers might inadequately delineate functional subtypes in certain contexts. To address this issue, we meticulously analyzed the transcriptomic profile of BMMs in a simplified co-culture system and demonstrated that, in the presence of Ti and BMSCs, BMMs underwent functional remodeling, transitioning from an M1-like to an M2-like phenotype. Additionally, BMSCs demonstrated augmented osteogenic capacity over time, consistent with previous studies [51–53]. In vivo, both M1-and M2-like BMM markers were upregulated on day 3 of post-implantation, likely reflecting an amplified immune response to the foreign body. As time progressed, the dominance shifted toward M2-like BMMs markers, suggesting an evolving milieu favoring M2-like macrophages during the bone tissue repair process. The distinctive functional molecules of M2-like BMMs appear to be influenced by the microenvironment, as detailed in the subsequent discussion.

Bioinformatic analysis of macrophages revealed a particular increase in chemokine secretion, including CXCL1, CXCL3, CXCL6, CXCL12, CXCL14, and CCL20. Subsequent experiments indicated that CXCL3, CXCL6, and CXCL14 were extracellularly secreted as signaling molecules, pivotal in orchestrating the phenotypic transformation of BMSCs. Our findings underscore the crucial role of CXCL chemokine-secreting M2-like BMMs in actively fueling BMSCs' osteogenic potential by activating their corresponding receptors, CXCR2 and CCR1. This insight

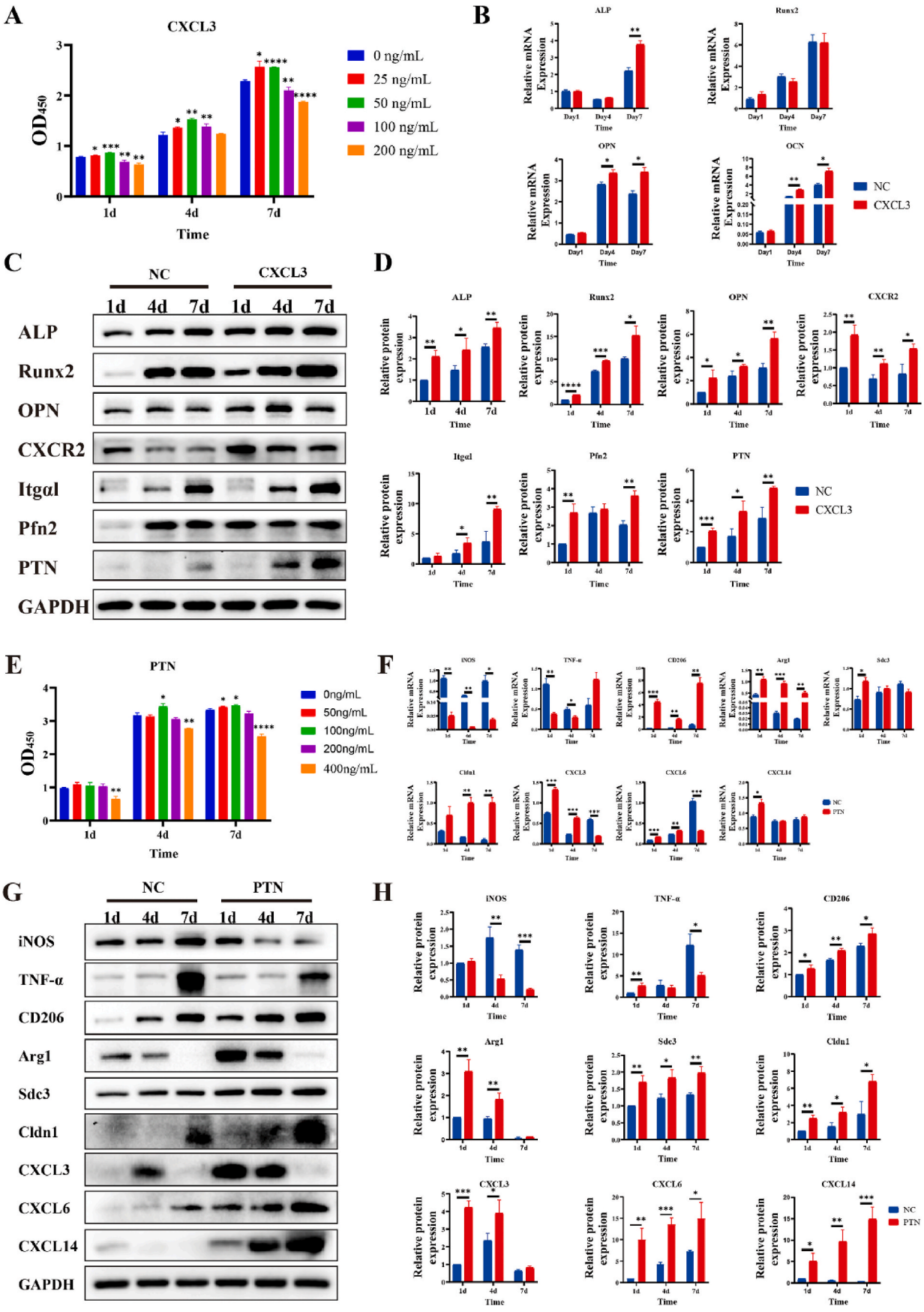

(caption on next page)

Fig. 7. Regulation of BMSCs and BMMs by CXCL3 and PTN. CXCL3 stimulates osteogenesis by binding to the CXCR2 receptor on BMSC surfaces, triggering activation of the downstream actin cytoskeleton pathway. Concurrently, PTN expression is elevated. PTN, when bound to Sdc3 on BMMs, drives macrophage differentiation through the CAM signaling pathway, consequently enhancing chemokine secretion. (A) The effect of varying concentrations of CXCL3 on BMSC proliferation over different time intervals, as determined using the CCK-8 kit. (B) CXCL3's impact on BMSC osteogenic differentiation, as assessed at the mRNA level across various time points. (C, D) CXCL3's effect on osteogenic differentiation and its associated molecular mechanisms in BMSCs, as analyzed at the protein level at different time points. (E) The effects of different concentrations of PTN on BMM proliferation at different time points, as detected using the CCK-8 kit. (F, G, H) The effects of PTN on BMMs differentiation as indicated by changes in the membrane receptors and downstream genes at the mRNA and protein levels and changes in the intracellular chemokine expression at various time points. Data are presented as mean ± SEM of at least three independent experiments. $^{*}p < 0.05$, $^{**}p < 0.01$, $^{***}p < 0.001$, and $^{****}p < 0.0001$. mRNA and protein expression were normalized to those of the NC group on day 1.

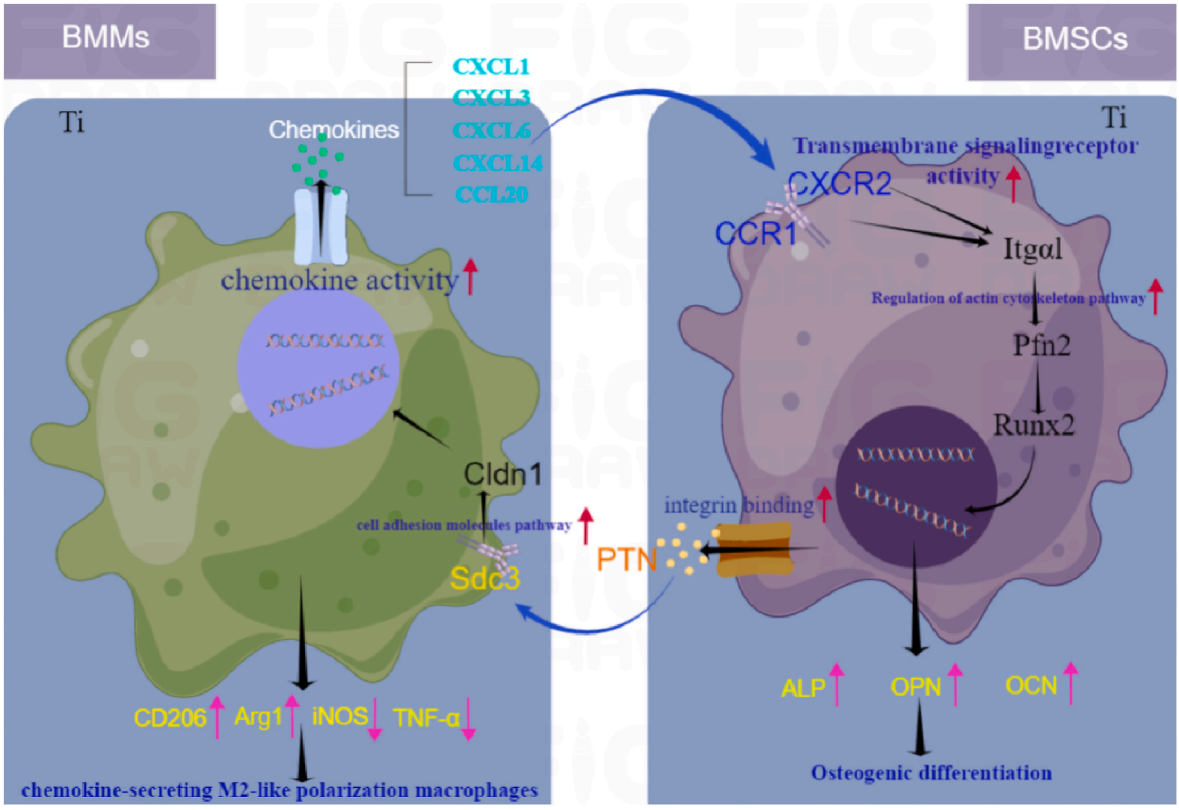

Fig. 8. Summary of the mechanisms underlying the interaction between BMMs and BMSCs after co-culture on titanium surfaces (Created by Figdraw: https://www.figdraw.com/).

could potentially reconcile the earlier discordant results regarding the impacts of the roughly categorized M2-like BMMs on osteointegration and osteogenic differentiation [20,47,54]. BMSCs, characterized by their pluripotent nature, have demonstrated the capacity to differentiate into a spectrum of tissue types, including cartilage, bone, muscle, and adipose tissue. Such differentiation is intricately steered by an array of cellular signals stemming from other cells in their microenvironment [55,56]. Chemokines, constituting a superfamily of small proteins, have been recognized as crucial players in immune and inflammatory responses [57,58] and bone metabolism [59–61]. Our study unveiled the presence of the corresponding receptors CXCR2 and CCR1 on the plasma membrane of BMSCs, thereby implicating their participation in promoting osteogenic differentiation via regulating the actin cytoskeleton pathway. This connection was substantiated through individual interventions with recombinant CXCL3, CXCL6, and CXCL14 proteins in BMSCs, revealing that not all chemokines exerted consistent osteogenic effects over time. Independent receptor agonistic experiments corroborated these osteogenesis-promoting effects, affirming that the communication between CXCL chemokine-secreting M2-like BMMs and BMSCs hinges on CXCL3, CXCL6, and CXCL14 binding to their respective receptors, CXCR2 and CCR1. This signaling cascade, in turn, culminated in activating the actin cytoskeleton pathway, leading to the up-regulation of Pfn2 expression, which subsequently increases the expression of osteogenesis-related genes.

Moreover, our findings suggest that BMSCs play a dual role; they not only act as osteogenic effector cells but also as regulators of BMMs' behaviors through feedback mechanisms. In the co-culture system, BMSCs differentially secreted PTN protein while exhibiting an osteogenic differentiation phenotype under the influence of extracellular cytokines. PTN was found to bind to Sdc3 receptor expressed on BMMs, orchestrating the phenotypic shift of BMMs through the CAM signaling pathway. Consequently, BMMs polarized towards an M2-like phenotype, accompanied by a chemokine secretion profile reminiscent of that observed in co-culture systems, indicating that PTN plays an important role in maintaining the M2-like phenotype of BMMs and regulating its cytokine secretion pattern as a feedback signal from BMSCs. Several studies have investigated the immune modulation of BMSCs and BMMs, with key molecules varying considerably in different prosthetic microenvironments [20,62–64]. We speculate that the feedback signals originating from BMSCs within specific environments vary, and their function is to maintain the system's stability, preventing excessive release of cytokines that could disrupt the microenvironment.

Dynamically modulated cell-cell communication mediated by cytokines was observed, with CXCL3, CXCL6, and CXCL14 emerging as

dominant factors at different time points. Analysis of transcription levels highlighted that, in comparison to the control group, the expression of CXCL1, CXCL3, CXCL6, CXCL14, and CCL20 secreted by BMMs in the co-culture system was significantly increased on day 1, CXCL1 and CXCL14 expression was augmented on day 4, and CXCL1 was increased on day 7. As time progressed, these chemokines gradually returned to the control levels, indicative of a feedback mechanism governing cytokine synthesis post-initial release. This regulatory feedback was shown to be mediated by PTN secreted by BMSCs. Moreover, protein analysis revealed that CXCL3 secretion was significantly increased on day 1, while CXCL6 was significantly increased on day 4 and day 7 and CXCL14 showed the highest increase on day 4. This dynamic pattern underscores the diverse impacts of different chemokines on BMSCs at various time points. Additionally, the expression of chemokine receptors in BMSCs remained relatively stable, with CCR1 (CXCL14 receptor) consistently elevated compared to the separate culture system across all time points. In contrast, the expression of CXCR2 (CXCL3 and CXCL6 receptor) remained stable except for day 7. This pattern may be attributed to BMSCs' role as effector cells that receive signals, with receptor regulation potentially exhibiting delayed responses beyond the observed time frame. Lastly, a similar dynamic shift was observed in PTN expression, starting from a peak and eventually returning to the control level. This further supports the notion that collaborative intercellular communication between BMMs and BMSCs constitutes a stable pro-osteogenesis microenvironment upon early interaction with Ti prosthesis.

In summary, this study established a new co-culture model that mirrors the immunological microenvironment after implantation in vivo. Our findings imply that CXCL chemokine-secreting M2-like BMMs are actively involved in BMSCs osteogenesis. We hypothesize that chemokines originating from BMMs, including CXCL3, CXCL6, and CXCL14, serve as primary messengers, initiating osteogenic differentiation through the downstream actin cytoskeleton pathway by activating CXCR2 and CCR1 receptors situated on the surface of BMSCs. Concurrently, BMSCs secrete PTN to orchestrate macrophage differentiation, thereby maintaining the M2-like phenotype via the receptor Sdc3-mediated cell adhesion molecules pathway. While further exploration is warranted to ascertain the complete scope of their interactions, our study sheds invaluable light on the crosstalk between BMSCs and BMMs on Ti surfaces and provides novel insights into the development of surface modification strategies for optimizing implant integration.

5. Conclusion

We explored the reciprocal communication between BMSCs and BMMs on Ti surfaces using an *in vitro* co-culture model. Under the influence of BMSCs, M2-like BMMs secrete CXCL chemokines. These chemokines bind to CXCR2 and CCR1 receptors on the surface of BMSCs, thereby triggering BMSCs' osteogenic differentiation through their downstream actin cytoskeleton pathway. Conversely, the interaction between BMSCs and BMMs results in the secretion of PTN by BMSCs. This PTN binds to its receptor Sdc3 on the surface of BMMs, inducing M2-like polarization of BMMs through the CAM signaling pathway.

Funding statement

This work was supported by the National Natural Science Foundation of China (No. 82072405 and No. 81571816)

Credit author statement

Yayun Zhang: Conceptualization, Methodology, Software, Writing-original draft. **Jiemao Wei:** Methodology, Writing-original draft. **Xingbang Yu:** Data curation, Writing- Original draft preparation. **Liangxi Chen:**Data curation. **Ranyue Ren**: Visualization, Investigation. **Yimin Dong:** Software. **Sibo Wang**: Validation. **Meipeng Zhu:** Visualization. **Nannan Ming:** Validation. **Ziwei Zhu:** Data curation. **Chenghao Gao:** Methodology, Supervision, Validation. **Wei Xiong:** Conceptualization, Writing- Reviewing and Editing.

Declaration of competing interest

On behalf of my co-authors, we have no financial or other relationships that might lead to a conflict of interest in the present article. All authors have reviewed the final version of the manuscript and approved it for publication.

Thank you and best regards.

Yours sincerely.

Wei Xiong

Jun 09 2023

Data availability

Data will be made available on request.

Appendix A. Supplementary data

Supplementary data to this article can be found online at https://doi.org/10.1016/j.mtbio.2023.100816.

References

[1] J.L. Wang, J.K. Xu, C. Hopkins, D.H. Chow, L. Qin, Biodegradable magnesium-based implants in orthopedics-A general review and perspectives, Adv. Sci. 7 (8) (2020), 1902443.
[2] J. Li, C. Zhao, Y. Xu, L. Song, Y. Chen, Y. Xu, Y. Ma, S. Wang, A. Xu, F. He, Remodeling of the osteoimmune microenvironment after biomaterials implantation in murine tibia: single-cell transcriptome analysis, Bioact. Mater. 22 (2023) 404–422.
[3] Y. Chen, M. Guan, R. Ren, C. Gao, H. Cheng, Y. Li, B. Gao, Y. Wei, J. Fu, J. Sun, W. Xiong, Improved immunoregulation of ultra-low-dose silver nanoparticle-loaded TiO(2) nanotubes via M2 macrophage polarization by regulating GLUT1 and autophagy, Int. J. Nanomed. 15 (2020) 2011–2026.
[4] J.G. Meyerink, D. Kota, S.T. Wood, G.A. Crawford, Transparent titanium dioxide nanotubes: processing, characterization, and application in establishing cellular response mechanisms, Acta Biomater. 79 (2018) 364–374.
[5] S. Guo, L.A. Dipietro, Factors affecting wound healing, J. Dent. Res. 89 (3) (2010) 219–229.
[6] M.C. Walsh, N. Kim, Y. Kadono, J. Rho, S.Y. Lee, J. Lorenzo, Y. Choi, Osteoimmunology: interplay between the immune system and bone metabolism, Annu. Rev. Immunol. 24 (2006) 33–63.
[7] M. Ponzetti, N. Rucci, Updates on osteoimmunology: what's new on the cross-talk between bone and immune system, Front. Endocrinol. 10 (2019) 236.
[8] R. Trindade, T. Albrektsson, P. Tengvall, A. Wennerberg, Foreign body reaction to biomaterials: on mechanisms for buildup and breakdown of osseointegration, Clin. Implant Dent. Relat. Res. 18 (1) (2016) 192–203.
[9] G.M. Keegan, I.D. Learmonth, C.P. Case, A systematic comparison of the actual, potential, and theoretical health effects of cobalt and chromium exposures from industry and surgical implants, Crit. Rev. Toxicol. 38 (8) (2008) 645–674.
[10] K. Ley, M1 means kill; M2 means heal, J. Immunol. 199 (7) (2017) 2191–2193.
[11] Z.G. Fridlender, J. Sun, S. Kim, V. Kapoor, G. Cheng, L. Ling, G.S. Worthen, S. M. Albelda, Polarization of tumor-associated neutrophil phenotype by TGF-beta: "N1" versus "N2" TAN, Cancer Cell 16 (3) (2009) 183–194.
[12] E. Olmsted-Davis, J. Mejia, E. Salisbury, Z. Gugala, A.R. Davis, A population of M2 macrophages associated with bone formation, Front. Immunol. 12 (2021), 686769.
[13] P. Zhou, D. Xia, Z. Ni, T. Ou, Y. Wang, H. Zhang, L. Mao, K. Lin, S. Xu, J. Liu, Calcium silicate bioactive ceramics induce osteogenesis through oncostatin M, Bioact. Mater. 6 (3) (2021) 810–822.
[14] T. Wang, J. Bai, M. Lu, C. Huang, D. Geng, G. Chen, L. Wang, J. Qi, W. Cui, L. Deng, Engineering immunomodulatory and osteoinductive implant surfaces via mussel adhesion-mediated ion coordination and molecular clicking, Nat. Commun. 13 (1) (2022) 160.
[15] Y. Feng, Q. Li, D. Wu, Y. Niu, C. Yang, L. Dong, C. Wang, A macrophage-activating, injectable hydrogel to sequester endogenous growth factors for in situ angiogenesis, Biomaterials 134 (2017) 128–142.
[16] B.N. Brown, J.E. Valentin, A.M. Stewart-Akers, G.P. McCabe, S.F. Badylak, Macrophage phenotype and remodeling outcomes in response to biologic scaffolds with and without a cellular component, Biomaterials 30 (8) (2009) 1482–1491.
[17] B.N. Brown, R. Londono, S. Tottey, L. Zhang, K.A. Kukla, M.T. Wolf, K.A. Daly, J. E. Reing, S.F. Badylak, Macrophage phenotype as a predictor of constructive remodeling following the implantation of biologically derived surgical mesh materials, Acta Biomater. 8 (3) (2012) 978–987.
[18] R.L. Shin, C.W. Lee, O.Y. Shen, H. Xu, O.K. Lee, The crosstalk between mesenchymal stem cells and macrophages in bone regeneration: a systematic review, Stem Cell. Int. 2021 (2021), 8835156.

[19] Z. Chen, C. Wu, W. Gu, T. Klein, R. Crawford, Y. Xiao, Osteogenic differentiation of bone marrow MSCs by beta-tricalcium phosphate stimulating macrophages via BMP2 signalling pathway, Biomaterials 35 (5) (2014) 1507–1518.
[20] P. Guihard, Y. Danger, B. Brounais, E. David, R. Brion, J. Delecrin, C.D. Richards, S. Chevalier, F. Redini, D. Heymann, H. Gascan, F. Blanchard, Induction of osteogenesis in mesenchymal stem cells by activated monocytes/macrophages depends on oncostatin M signaling, Stem Cell. 30 (4) (2012) 762–772.
[21] D.O. Freytes, J.W. Kang, I. Marcos-Campos, G. Vunjak-Novakovic, Macrophages modulate the viability and growth of human mesenchymal stem cells, J. Cell. Biochem. 114 (1) (2013) 220–229.
[22] S. Hosseinpour, L.J. Walsh, C. Xu, Modulating osteoimmune responses by mesoporous silica nanoparticles, ACS Biomater. Sci. Eng. 8 (10) (2022) 4110–4122.
[23] O. Veiseh, J.C. Doloff, M. Ma, A.J. Vegas, H.H. Tam, A.R. Bader, J. Li, E. Langan, J. Wyckoff, W.S. Loo, S. Jhunjhunwala, A. Chiu, S. Siebert, K. Tang, J. Hollister-Lock, S. Aresta-Dasilva, M. Bochenek, J. Mendoza-Elias, Y. Wang, M. Qi, D. M. Lavin, M. Chen, N. Dholakia, R. Thakrar, I. Lacik, G.C. Weir, J. Oberholzer, D. L. Greiner, R. Langer, D.G. Anderson, Size- and shape-dependent foreign body immune response to materials implanted in rodents and non-human primates, Nat. Mater. 14 (6) (2015) 643–651.
[24] W. Qiao, D. Pan, Y. Zheng, S. Wu, X. Liu, Z. Chen, M. Wan, S. Feng, K.M.C. Cheung, K.W.K. Yeung, X. Cao, Divalent metal cations stimulate skeleton interoception for new bone formation in mouse injury models, Nat. Commun. 13 (1) (2022) 535.
[25] A.T. Xu, Y.W. Xie, J.G. Xu, J. Li, H. Wang, F.M. He, Effects of strontium-incorporated micro/nano rough titanium surfaces on osseointegration via modulating polarization of macrophages, Colloids Surf. B Biointerfaces 207 (2021), 111992.
[26] F. da Silva Lima, A.B. da Rocha Romero, A. Hastreiter, A. Nogueira-Pedro, E. Makiyama, C. Colli, R.A. Fock, An insight into the role of magnesium in the immunomodulatory properties of mesenchymal stem cells, J. Nutr. Biochem. 55 (2018) 200–208.
[27] M. Tsukasaki, H. Takayanagi, Osteoimmunology: evolving concepts in bone-immune interactions in health and disease, Nat. Rev. Immunol. 19 (10) (2019) 626–642.
[28] E.M. O'Brien, G.E. Risser, K.L. Spiller, Sequential drug delivery to modulate macrophage behavior and enhance implant integration, Adv. Drug Deliv. Rev. 149–150 (2019) 85–94.
[29] K. English, Mechanisms of mesenchymal stromal cell immunomodulation, Immunol. Cell Biol. 91 (1) (2013) 19–26.
[30] L. Gong, Y. Zhao, Y. Zhang, Z. Ruan, The macrophage polarization regulates MSC osteoblast differentiation in vitro, Ann. Clin. Lab. Sci. 46 (1) (2016) 65–71.
[31] W. Shang, G. Chen, Y. Li, Y. Zhuo, Y. Wang, Z. Fang, Y. Yu, H. Ren, Static magnetic field accelerates diabetic wound healing by facilitating resolution of inflammation, J. Diabetes Res. 2019 (2019), 5641271.
[32] J. Pajarinen, T. Lin, E. Gibon, Y. Kohno, M. Maruyama, K. Nathan, L. Lu, Z. Yao, S. B. Goodman, Mesenchymal stem cell-macrophage crosstalk and bone healing, Biomaterials 196 (2019) 80–89.
[33] M. Jiao, R. Tian, G. Liu, X. Liu, Q. Wei, J. Yan, K. Wang, P. Yang, Circular RNA and messenger RNA expression profile and competing endogenous RNA network in subchondral bone in osteonecrosis of the femoral head, DNA Cell Biol. 40 (1) (2021) 61–69.
[34] J. Lee, M.J. Cuddihy, N.A. Kotov, Three-dimensional cell culture matrices: state of the art, Tissue Eng., Part B 14 (1) (2008) 61–86.
[35] T.M. Blanco, A. Mantalaris, A. Bismarck, N. Panoskaltsis, The development of a three-dimensional scaffold for ex vivo biomimicry of human acute myeloid leukaemia, Biomaterials 31 (8) (2010) 2243–2251.
[36] G. Valles, F. Bensiamar, L. Crespo, M. Arruebo, N. Vilaboa, L. Saldana, Topographical cues regulate the crosstalk between MSCs and macrophages, Biomaterials 37 (2015) 124–133.
[37] D.W. Lee, J. Kang, H.J. Hwang, M.S. Oh, B.C. Shin, M.Y. Lee, H.J. Kuh, Pitch-tunable pillar arrays for high-throughput culture and immunohistological analysis of tumor spheroids, RSC Adv. 8 (9) (2018) 4494–4502.
[38] H.J. Hwang, M.S. Oh, D.W. Lee, H.J. Kuh, Multiplex quantitative analysis of stroma-mediated cancer cell invasion, matrix remodeling, and drug response in a 3D co-culture model of pancreatic tumor spheroids and stellate cells, J. Exp. Clin. Cancer Res. 38 (1) (2019) 258.
[39] H. Tang, J.F.A. Husch, Y. Zhang, J.A. Jansen, F. Yang, J. van den Beucken, Coculture with monocytes/macrophages modulates osteogenic differentiation of adipose-derived mesenchymal stromal cells on poly(lactic-co-glycolic) acid/polycaprolactone scaffolds, J Tissue Eng Regen Med 13 (5) (2019) 785–798.
[40] X.T. He, X. Li, Y. Yin, R.X. Wu, X.Y. Xu, F.M. Chen, The effects of conditioned media generated by polarized macrophages on the cellular behaviours of bone marrow mesenchymal stem cells, J. Cell Mol. Med. 22 (2) (2018) 1302–1315.
[41] R.R. Miranda, A.L. Damaso da Silveira, I.P. de Jesus, S.R. Grotzner, C.L. Voigt, S. X. Campos, J.R. Garcia, M.A. Randi, C.A. Ribeiro, F. Filipak Neto, Effects of realistic concentrations of TiO(2) and ZnO nanoparticles in Prochilodus lineatus juvenile fish, Environ. Sci. Pollut. Res. Int. 23 (6) (2016) 5179–5188.
[42] D. Bello, D.B. Warheit, Biokinetics of engineered nano-TiO(2) in rats administered by different exposure routes: implications for human health, Nanotoxicology 11 (4) (2017) 431–433.
[43] N.A. Hodges, E.M. Sussman, J.P. Stegemann, Aseptic and septic prosthetic joint loosening: impact of biomaterial wear on immune cell function, inflammation, and infection, Biomaterials 278 (2021), 121127.
[44] R.D. Stout, C. Jiang, B. Matta, I. Tietzel, S.K. Watkins, J. Suttles, Macrophages sequentially change their functional phenotype in response to changes in microenvironmental influences, J. Immunol. 175 (1) (2005) 342–349.
[45] J. Kim, P. Hematti, Mesenchymal stem cell-educated macrophages: a novel type of alternatively activated macrophages, Exp. Hematol. 37 (12) (2009) 1445–1453.
[46] F.O. Martinez, L. Helming, S. Gordon, Alternative activation of macrophages: an immunologic functional perspective, Annu. Rev. Immunol. 27 (2009) 451–483.
[47] W. He, H. Che, C. Jin, Y. Li, F. Li, R. Zhou, LncRNA AFAP1-AS1 promotes M1 polarization of macrophages and osteogenic differentiation of valve interstitial cells, J. Physiol. Biochem. 77 (3) (2021) 461–468.
[48] K.L. Spiller, T.J. Koh, Macrophage-based therapeutic strategies in regenerative medicine, Adv. Drug Deliv. Rev. 122 (2017) 74–83.
[49] J. Wang, D. Liu, B. Guo, X. Yang, X. Chen, X. Zhu, Y. Fan, X. Zhang, Role of biphasic calcium phosphate ceramic-mediated secretion of signaling molecules by macrophages in migration and osteoblastic differentiation of MSCs, Acta Biomater. 51 (2017) 447–460.
[50] F. Zhao, W. Xie, W. Zhang, X. Fu, W. Gao, B. Lei, X. Chen, 3D printing nanoscale bioactive glass scaffolds enhance osteoblast migration and extramembranous osteogenesis through stimulating immunomodulation, Adv. Healthcare Mater. 7 (16) (2018), e1800361.
[51] G.S. Boersema, N. Grotenhuis, Y. Bayon, J.F. Lange, Y.M. Bastiaansen-Jenniskens, The effect of biomaterials used for tissue regeneration purposes on polarization of macrophages, Biores Open Access 5 (1) (2016) 6–14.
[52] J. Maggini, G. Mirkin, I. Bognanni, J. Holmberg, I.M. Piazzon, I. Nepomnaschy, H. Costa, C. Canones, S. Raiden, M. Vermeulen, J.R. Geffner, Mouse bone marrow-derived mesenchymal stromal cells turn activated macrophages into a regulatory-like profile, PLoS One 5 (2) (2010), e9252.
[53] J. Wang, J. Xia, R. Huang, Y. Hu, J. Fan, Q. Shu, J. Xu, Mesenchymal stem cell-derived extracellular vesicles alter disease outcomes via endorsement of macrophage polarization, Stem Cell Res. Ther. 11 (1) (2020) 424.
[54] J.R. Alhamdi, T. Peng, I.M. Al-Naggar, K.L. Hawley, K.L. Spiller, L.T. Kuhn, Controlled M1-to-M2 transition of aged macrophages by calcium phosphate coatings, Biomaterials 196 (2019) 90–99.
[55] G. Ren, L. Zhang, X. Zhao, G. Xu, Y. Zhang, A.I. Roberts, R.C. Zhao, Y. Shi, Mesenchymal stem cell-mediated immunosuppression occurs via concerted action of chemokines and nitric oxide, Cell Stem Cell 2 (2) (2008) 141–150.
[56] G. Borciani, G. Montalbano, N. Baldini, G. Cerqueni, C. Vitale-Brovarone, G. Ciapetti, Co-culture systems of osteoblasts and osteoclasts: simulating in vitro bone remodeling in regenerative approaches, Acta Biomater. 108 (2020) 22–45.
[57] A. Mantovani, The chemokine system: redundancy for robust outputs, Immunol. Today 20 (6) (1999) 254–257.
[58] A. Mantovani, A. Sica, S. Sozzani, P. Allavena, A. Vecchi, M. Locati, The chemokine system in diverse forms of macrophage activation and polarization, Trends Immunol. 25 (12) (2004) 677–686.
[59] C.C. Biguetti, F. Cavalla, E.M. Silveira, A.C. Fonseca, A.E. Vieira, A.P. Tabanez, D. C. Rodrigues, A.P.F. Trombone, G.P. Garlet, Oral implant osseointegration model in C57Bl/6 mice: microtomographic, histological, histomorphometric and molecular characterization, J. Appl. Oral Sci. 26 (2018), e20170601.
[60] H.M. Ko, J.S. Moon, H.K. Shim, S.Y. Lee, J.H. Kang, M.S. Kim, H.J. Chung, S. H. Kim, Inhibitory effect of C-X-C motif chemokine ligand 14 on the osteogenic differentiation of human periodontal ligament cells through transforming growth factor-beta1, Arch. Oral Biol. 115 (2020), 104733.
[61] Y. Chen, H. Wang, Q. Yang, W. Zhao, Y. Chen, Q. Ni, W. Li, J. Shi, W. Zhang, L. Li, Y. Xu, H. Zhang, D. Miao, L. Xing, W. Sun, Single-cell RNA landscape of the osteoimmunology microenvironment in periodontitis, Theranostics 12 (3) (2022) 1074–1096.
[62] J.H. Ylostalo, T.J. Bartosh, K. Coble, D.J. Prockop, Human mesenchymal stem/stromal cells cultured as spheroids are self-activated to produce prostaglandin E2 that directs stimulated macrophages into an anti-inflammatory phenotype, Stem Cell. 30 (10) (2012) 2283–2296.
[63] S.N. King, S.E. Hanson, X. Chen, J. Kim, P. Hematti, S.L. Thibeault, In vitro characterization of macrophage interaction with mesenchymal stromal cell-hyaluronan hydrogel constructs, J. Biomed. Mater. Res. 102 (3) (2014) 890–902.
[64] M.E. Bernardo, W.E. Fibbe, Mesenchymal stromal cells: sensors and switchers of inflammation, Cell Stem Cell 13 (4) (2013) 392–402.